Powder Technology 320 (2017) 285–294

Contents lists available at ScienceDirect

Powder Technology

journal homepage: www.elsevier.com/locate/powtec

Numerical study on deposition of particles in a 90° bend in the presence of swirling flow using Eulerian-Lagrangian method

Akbar Arsalanloo *, Majid Abbasalizadeh

Department of Mechanical Engineering, Faculty of Engineering, Urmia University, Urmia, Iran

ARTICLE INFO

Article history:
Received 16 February 2017
Received in revised form 11 July 2017
Accepted 17 July 2017
Available online 21 July 2017

ABSTRACT

An Eulerian-Lagrangian method has been used to study deposition and penetration of particles in a 90° bend in the presence of swirling flow. Presence of bends and curved pipes is inevitable for industrial applications and deposition of particles in curved pipes is a commonplace phenomenon and may reduce system efficiency or cause erosion on the bend wall. The main objective of this study is to understand if deposition of particles is affected by imposing swirl to fluid flow. The simulations are performed using commercial CFD code Ansys Fluent and RSM turbulent model is employed for all simulations. Swirl was generated using internal spiral vanes which were placed on the inner wall of the pipe. Different heights for vanes and different swirling pitches were used to see how they affect swirl intensity and deposition efficiency. Deposition efficiency is reported as function of particle stokes number. It was found that both lowering swirling pitch and increasing vanes' heights increase swirl intensity and higher swirl intensities reduce deposition rates for wide range of stokes numbers. The results show that increasing vanes' heights have better effect on reduction of deposition efficiency than lowering swirling pitch. Another important finding of this study was that larger particles with higher stokes numbers have more predictable behavior in swirling flow and all ranges of swirl intensities reduce deposition rate of these particles.

1. Introduction

Conveying of aerosols as a dispersed phase in a continuous phase such as air and deposition of aerosols is an inevitable incident in a wide range of industrial and engineering processes. For example in air ventilation systems, deposition of aerosols in ducts or bends may block air flow and cause malfunction or reduce system efficiency. Air pollution and the suspended aerosols in the atmosphere is another field for studying about aerosols. Because of the similarities of multiphase flow patterns in a curved pipe or bend and human respiratory system, recognizing characteristic of particle deposition and conveying in carrying media has a key role for studying about inhaled pollutants and delivery of pharmaceutical aerosols in lungs and respiratory system. These few examples mentioned above show that studying about conveying and deposition of particles in pipelines and bends can play significant role in many scientific and engineering applications and many researchers have addressed this issue in the past years.

In 1973 Liu and Agarwal [1] experimentally measured deposition rate of particles in a vertical pipe for Reynolds numbers of ranging from 10,000 to 50,000 and Yang [2] worked on pneumatic conveying in vertical pipelines and correlated vertical velocity of particles. In the studies about conveying and deposition of particles, both laminar [3,4] and turbulent flow regimes [5,6] have been included.

Bends and curved pipes are very frequently used in mechanical systems. The centrifugal force exerted on fluid in curved pipes results in secondary flows which is called Dean vortices. Particle deposition or penetration through curved pipes is influenced by the streamline curvature of the fluid flow which indicates that studying on secondary flows is important in order to have a valid prediction of particle motions. Cheng and Wang [7] used theoretical calculations to predict trajectories of particles in a fully developed laminar flow. Pui et al. [8] experimentally investigated deposition efficiency of liquid particles in a bend with circular cross section in Reynolds numbers of ranging from 100 to 10,000 for different curvature ratios and found a correlation for deposition efficiency as a function of stokes number. Because rectangular duct bends are commonplace in a variety of engineering applications such as ventilation systems, some researchers have focused on predicting behavior of particles in rectangular duct bends [9–11]. Breuer et al. [12] applied LES model for predicting particle deposition in a 90° bend. Zhang et al. [13] employed different turbulent models with different near wall treatments to study deposition efficiency associated with different bend angles and curvature ratios for different flow Reynolds numbers. Li et al. [14] studied on deposition of particles in a 180° bend. Kevin et al. [15] studied particle collision and breakage in bends. Pipe bends are highly susceptible to wear and erosion as a result of particle impact on bends and has been addressed in several investigations [16,17]. Macchini et al. [18] focused on the effect of particle size,

* Corresponding author.
E-mail addresses: st_a.arsalanloo@urmia.ac.ir, akbar.arsalan89@gmail.com (A. Arsalanloo).

http://dx.doi.org/10.1016/j.powtec.2017.07.050
0032-5910/

Nomenclature

Roman letters

C_D	particle drag coefficient
C_p	pressure coefficient
d_p	particle diameter (m)
d	pipe diameter (m)
g	gravity acceleration (m/s^2)
h	spiral vanes' height (m)
L	entrance length (m)
L_s	characteristic length scale (m)
P	swirling pitches (m)
P_l	local static pressure (Pa)
P_∞	reference static pressure (Pa)
R	pipe radius (m)
R_b	bend radius (m)
Re	flow Reynolds number
Re_r	particle Reynolds number
S_n	swirl number
St	stokes number
u	air velocity (m/s)
u_p	particle velocity (m/s)
u_∞	reference velocity (m/s)
u_τ	frictional velocity (m/s)
v	axial velocity (m/s)
V_s	characteristic velocity (m/s)
w	tangential velocity (m/s)
y	distance of first cell centroid from wall (m)
y^+	dimensionless distance from wall

Greek letters

ρ_p	particle density (kg/m^3)
δ	curvature ratio
μ	dynamic viscosity of air (kg/m-s)
ρ	air density (kg/m^3)
τ_D	particle response time (s)
μ_t	eddy viscosity (kg/m-s)
τ_s	system response time (s)
η	deposition efficiency
v	kinematic viscosity (m^2/s)
τ_w	wall shear stress (Pa)
θ	bend deflection angle

Acronyms

DPM	discrete phase model
DRWM	discrete random walk model
EWT	enhanced wall treatment
LES	large eddy simulation
PDE	partial differential equation
PRESTO	pressure staggering option
RANS	Reynolds-averaged Navier-Stokes
RSM	Reynolds stress model

density and particle concentration on bend erosion. Researchers have addressed different aspects of particle conveying and its deposition in bends. The extent of literature available in this field indicates its importance in engineering and industrial applications. However this study aims to address new aspects of this issue.

Swirling flow is used in many applications such as cyclone separators [19], for separating aerosols from air or for increasing thermal efficiency in heat exchangers [20]. Rocha et al. [21] numerically and experimentally studied swirling flow generated by a fixed-guided vane-type swirl generator and Zhou et al. [22] compared three types of swirl generators used in pneumatic conveying systems in swirling intensity, pressure drop and swirl decaying rate.

Information about pneumatic conveying in pipelines and deposition of particles in bends has been widely presented in the literature. There are also more information about swirling flow at straight pipes and bends. However the main objective of the present work is to investigate deposition of particles in a 90° bend in the presence of swirling flow. Li [23] experimentally investigated swirling flow pneumatic conveying of particles in a 90° bend for Reynolds number of about 50,000 and 100,000 for micron-sized particles. The results of experiments showed that swirling flow can reduce impact of particles at pipe bend. In the present study deposition efficiency in a 90° bend with imposed swirling flow for Reynolds number of 10,000 and particle diameters of 2 to 9 μm has been numerically investigated. After validating the model with the experimental work of Pui et al. swirl has been imposed to the flow using internal spiral vanes with different pitch lengths and various heights to create different swirl intensities. Deposition efficiency has been reported as a function of stokes number and also the flow patterns and its deflection as a result of swirl has been displayed along pipe axis.

2. Numerical simulation

2.1. Physical model and problem statement

Deposition of particles in a 90° bend is simulated using an Eulerian-Lagrangian method. Deposition efficiency was calculated in a simple pipe with a 90° bend to validate the model using experimental data provided by Pui et al. [8]. They studied deposition of droplets in a 90° bend being carried by air. Their study contained pipes of different diameters, curvature ratios and different flow Reynolds numbers and included various materials for test pipes. After validating the model, internal spiral vanes were mounted on the inner wall of tube as a swirl generator and effect of swirling flow entering the bend, on deposition efficiency was investigated at different swirl intensities. A 2D schematic of the model is shown in Fig. 1. The particles were injected at an upstream distance of 2d from the bend entrance. Injections were performed in a square region with sides of 0.3d located at the middle of the pipe to avoid trapping of particles on pipe wall before they have the chance to enter the bend. A long entrance length has been chosen for pipe based on the equation presented by Munson [24] to ensure that the flow is fully developed before entering the bend.

$$\frac{L}{d} = 4.4\,Re^{1/6} \tag{1}$$

where L is entrance length, d is pipe diameter and *Re* is the flow Reynolds number.

After the model was validated, spiral vanes were placed on the pipe wall with the length of 0.15 m long before the bend entrance. Different swirling pitches and different heights for vanes were used to see how they affect swirling intensity and to verify the possibility of any relation between swirl intensity and deposition rate. The heights of vanes were ranging from h/d = 0.05 to 0.35 and swirling pitches with $P = 0.15, 0.1, 0.075$, 0.05 m were used for the study. Fig. 2 displays a 3D view of pipe including swirling section and the positions of spiral vans on pipe wall. All the computations were performed for Reynolds number of 10,000 with a pipe diameter of d = 8.51 mm and curvature ratio of $(\delta = \frac{R_b}{R})$ δ = 5.6. Velocity inlet and pressure outlet boundary conditions were used for pipe inlet and outlet and a "no slip" boundary condition was set for the pipe wall.

2.2. Grid generation and mesh independence study

For mesh independence study and validation, O-type structural mesh was used for one cross section and it was swept with mesh, along the pipe axis to create structural hexahedral mesh for the entire

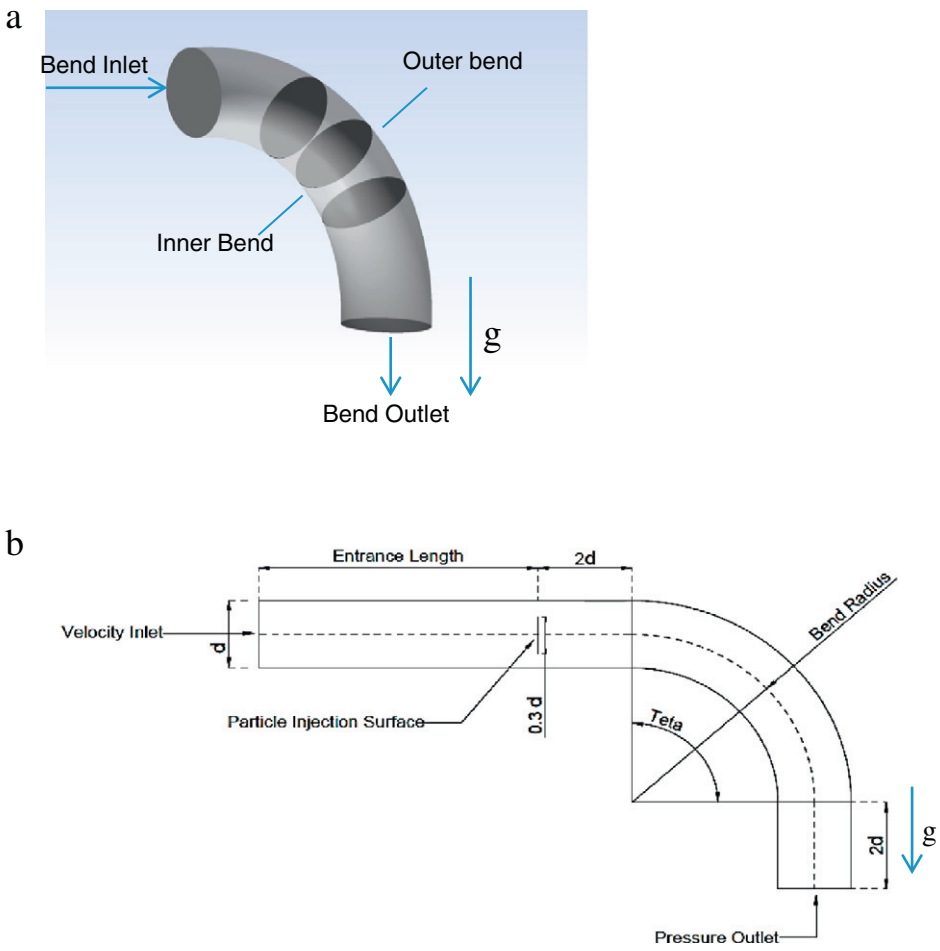

Fig. 1. Schematic view of model: (a) 3D view of bend and placement of planes at $\theta = 0^{\circ}, 30^{\circ}, 45^{\circ}, 60^{\circ}, 90^{\circ}$. (b) 2D view of the model with locations of the velocity inlet and pressure outlet boundary conditions.

computational domain. Details of meshes created for independence study are presented in Table 1. After the spiral vanes were mounted on the inner wall of the pipe, the swirling section was meshed with quadrilateral paved mesh and an O-type structured mesh was used for rest of the computational domain. For the surfaces with different mesh topologies to be recognized by CFD code Ansys Fluent, the interface boundary condition was used to connect inlet and outlet of swirling section to rest of computational domain. Fig. 3 depicts a cross sectional view of structured and paved meshes used.

Before running any simulation, a mesh independence study was performed to ensure maximum validity of grids generated. To do so, six geometries with 30,000, 67,000, 122,000, 320,000, 560,000 and 990,000 cells were created. Deposition efficiency for particles with st = 0.85 was tested for each mesh. The results for independence study are shown in Fig. 4. As shown in this figure, increasing number of grids from 320,000 to 560,000 makes no significant change to deposition efficiency and the results are independent from the mesh. However in spite of difference in results, some of the parameters for mesh quality such as aspect ratio and skewness of grids, was taken into account. After due considerations the mesh with 560,000 grids was determined to be have the best quality required so it was chosen for performing simulations.

2.3. Continuous phase

An Eulerian approach has been used to simulate the continuous phase. Air is used as the carrying media with density of $\rho = 1.225$ kg/m^3. As air Mach number is <0.3, due to the assumption of steady state and isothermal flow, we can consider air as incompressible flow therefore a pressure based solver was used in the computations. To stabilize the solution, Under-Relaxation Factors were reduced (0.2 for pressure and 0.5 for

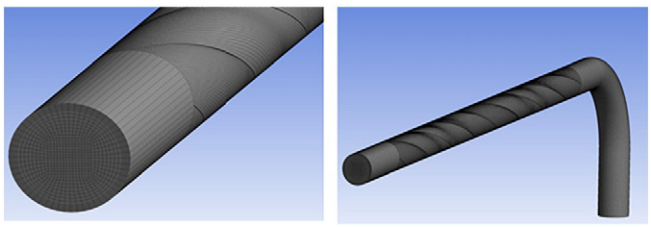

Fig. 2. 3D view of the computational domain including swirl section.

Table 1
details of meshes used for mesh independence study.

	Number of cross sections along the pipe axis	Number of grids for each cross section	Total number of grids	Total number of nodes
1	162	185	29,970	31,948
2	244	276	67,344	70,805
3	244	500	122,000	127,645
4	489	672	328,608	341,530
5	611	924	564,564	583,236
6	816	1216	992,256	1,020,433

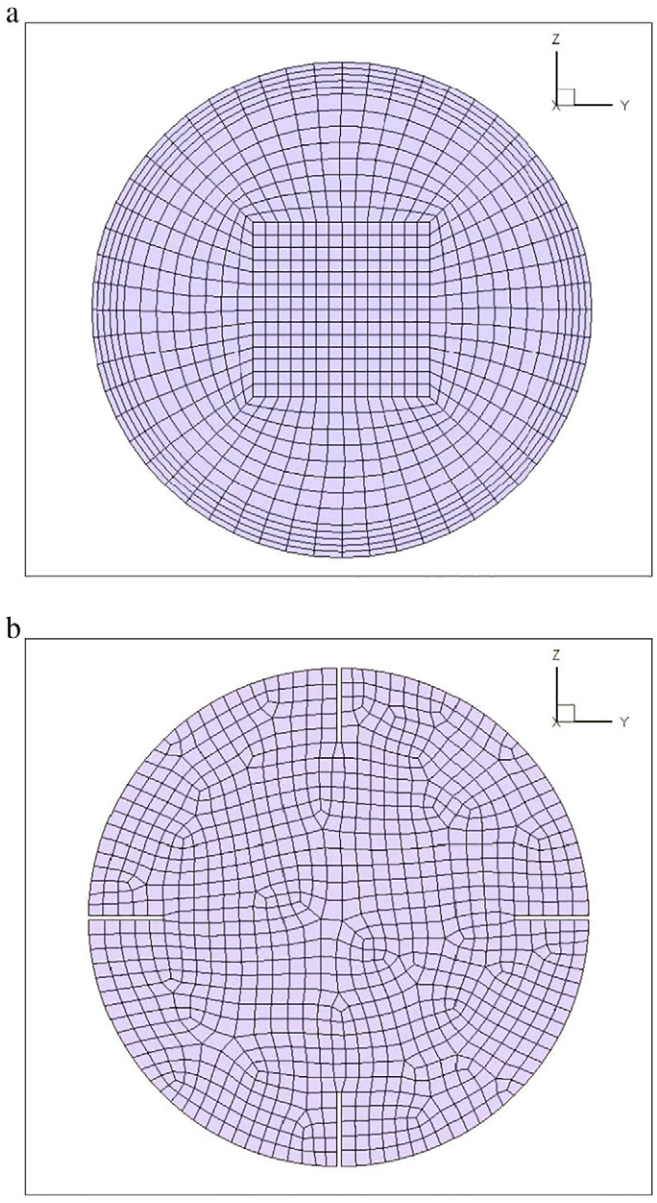

Fig. 3. Cross sectional view of mesh used for model: (a) O-type structured mesh with boundary layer mesh near the wall region, (b) unstructured paved mesh used in the swirl section.

momentum). PRESTO! has been used as pressure interpolation scheme which gives more accurate results for swirling flows and flows with streamline curvature. Momentum, dissipation rate and kinetic energy equations have been discretized with Second Order Upwind scheme and the SIMPLE method is used for pressure-velocity coupling. For all variables 10^{-7} is set as the residual criterion for residuals' convergence.

2.3.1. Turbulence modeling

Ansys Fluent package covers different models for predicting turbulent flow regimes. To choose an appropriate turbulence model several factors must be considered such as physical situations governing the flow being modeled, level of accuracy required and available CPU and computer resources. The most frequently used turbulent models for engineering applications are the eddy-viscosity models which are based on the Boussinesq hypothesis. It states that the Reynolds stresses appeared in the RANS (Reynolds averaged Navier Stokes) equations can be related to the mean velocity gradients using the concept of eddy-viscosity (μ_t) often called as turbulent viscosity. This theory assumes the turbulent

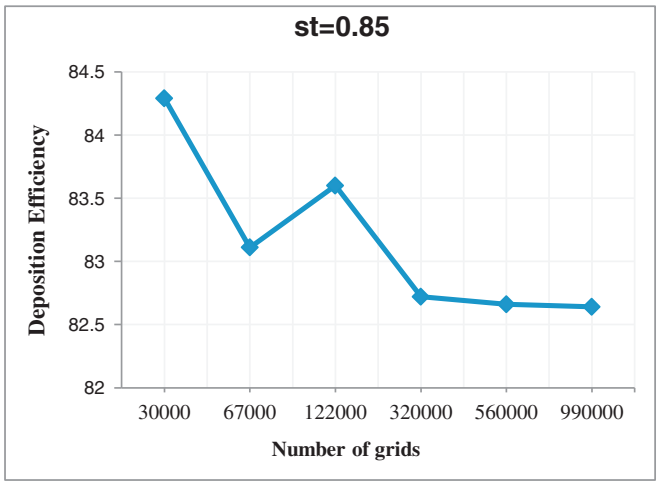

Fig. 4. Deposition Efficiency of particles with st = 0.85 for six different meshes produced.

viscosity as an isotropic scalar quantity. This assumption significantly lowers the computational costs but offers poor prediction for flows containing anisotropic turbulence fluctuations such as flows with strong separation, highly swirling and rotating flows, flows with large streamline curvatures and large pressure gradients. Unlike k-ε, Reynolds stress model is not a low-cost model as it avoids the isotropic eddy-viscosity assumption and solves six transport equation for Reynolds stresses and an extra transport equation for the dissipation rate which increases computational costs by solving 5 PDE equations more than k-ε, but can effectively capture features of flow resulted from anisotropy of turbulence. However because in this study swirling flow in the presence of streamline curvature is being modeled, RSM can provide more accurate results than any of the eddy-viscosity models so RSM has been chosen to run the simulations.

2.3.2. Modeling near wall region

Near wall regions are important for CFD simulations, since solution variables are prone to large gradients in that region. Viscous effects have major role on flow variables in the near wall area but as moving away from the wall toward the turbulent core, inertial effects play the dominant role. Fluent uses methods of “Wall Functions” and “EWT” for modeling flow in the near wall region. “Wall functions” doesn't completely solve flow field near the wall but instead uses empirical formulas to connect the parameters of flow in the viscosity affected region to the turbulent core however “EWT” resolves the flow field all the way down to the wall [25]. The dimensionless distance ($y^+ = \frac{yu_\tau}{\nu}$) is used to state the mesh resolution requirements for each method where y is the distance from wall to the first cell centroid adjacent to the wall, u_τ is the friction velocity defined as $\sqrt{\frac{\tau_w}{\rho}}$ and ν is kinematic viscosity. As recommended by fluent user's guide, for wall functions method the first cell centroid should be located in the $30<y^+<300$ region and for EWT this parameter must be on the order of $y^+ \sim 1$. EWT accurately captures boundary layer turbulence but needs finer meshes for boundary layer but the wall functions on the other hand, result in lower mesh resolution and therefore lower computational cost and is reliable when modeling the near wall effects is not our first priority.

Despite economic advantages of wall functions, there are several limitations for using these methods. Large pressure gradients, boundary layer separation and inclined streamlines (high 3 dimensionality near the wall) are major conditions that cause erroneous results. As in this work parameters of flow near the wall directly affect deposition rate, EWT has been used in this research to avoid the potential shortcomings of wall functions as mentioned and the near wall meshes have been

refined to meet the requirements for y^+ as recommended by Ansys Fluent user's guide.

2.3.3. Swirl number

Swirl number is a dimensionless parameter used to express swirl intensity in swirling flow and is widely used in many researches since 1980s [26]. In the present study swirl number has been used to indicate effects of spiral vanes on swirl intensity and effect of swirling flow on particle deposition. It is defined as the ratio of the axial flux of angular momentum to the axial flux of axial momentum on a desired surface:

$$S_n = \frac{\int \rho w v . dA}{R \int \rho u v . dA} \tag{2}$$

where v is axial velocity, w is tangential velocity and R is the pipe radius.

To calculate this parameter, the nominator and denominator must be calculated separately in the software. To calculate nominator, the term radius * tangential-velocity must be defined in the user defined functions and flowrate of this function must be calculated in the software over the intended surface. Finally the swirling number is achieved by calculating the following proportion:

$$S_n = \frac{Flowrate\ (r^* w)}{R^* Flowrate(v)}$$

2.4. Discrete phase

The volume fraction for the dispersed phase is much <10% of the volume fraction for the continuous phase and it is assumed that there is no particle-particle interaction and that trajectories of discrete phase do not impact continuous phase flow patterns, therefore a one way coupling Discrete Phase Model is employed. In DPM, trajectory of particles is predicted by integrating the equation of motion for every particle which is in a Lagrangian frame of reference and can be written as:

$$\frac{du_p}{d_t} = F_D(u - u_p) + \frac{g\left(\rho_p - \rho\right)}{\rho_p} \tag{3}$$

where

$$F_D = \frac{18\mu}{\rho_p {d_p}^2} \frac{C_D Re_r}{24} \tag{4}$$

and

$$Re_r = \frac{\rho d_p \left|u_p - u\right|}{\mu} \tag{5}$$

In the above equations, du/dt is the particle inertia, $FD(u - up)$ is the drag force per unit particle mass, $\frac{g(\rho_p - \rho)}{\rho_p}$ is the buoyancy force per unit particle mass, ρ is the fluid density, ρ_p is the density of particle, d_p is particle diameter, u is fluid velocity, u_p is particle velocity, g is the gravity acceleration, Re_r is the relative Reynolds number (particle Reynolds number), C_D is the particle drag coefficient which is defined as [27]

$$C_d = \frac{24}{Re_r} \tag{6}$$

for $Re_r < 1$ and for $1 < Re_r < 400$ C_D is defined as:

$$C_D = \frac{24}{Re_r}^* \left(1 + 0.15 {Re_r}^{0.687}\right) \tag{7}$$

and μ is the dynamic viscosity of fluid. As the particles are assumed spherical, the spherical drag law is employed to calculate drag force.

Other forces may affect particle motion in some specific circumstances that should be included in the particle equation of motion. In case of submicron particles, the random motion of particles which is called Brownian motion importantly affects velocity of particles and their direction but as diameter of particles simulated is above 1 μm so the Brownian force is not included in Eq. (3). Saffman's Lift Force is another force that can be important in case of submicron particles as recommended by Ansys Fluent user's guide but based on aforementioned reasons this force is neglected too. Presence of temperature gradient in a flow exerts a force on the dispersed phase in the opposite direction of the gradient. This force is called thermophoretic force. As there is no temperature gradient in this work, this force also is not included in the particle motions equation. As a conclusion the drag force and buoyancy force are the only forces included in the equation of motion of particles.

About 25,000 particles with density of 895 kg/m^3 have been injected from a surface with upstream distance of 2d from the bend entrance. The injection position has been shown schematically in Fig. 1b. The initial injection velocity of particles was set to be equal to the mean axial flow velocity of air at the injection section. Minimum particle diameter is 2.98 μm and the maximum particle diameter is 9.67 μm which are associated with stokes numbers of 0.1 and 1.05 respectively. Particles are assumed to be rigid and experience no deformation or break up in the simulations. It is assumed that when particles reach the wall adhere to it and there is no particle reflection from the surface which is compatible with the experimental method of Pui et al. so boundary condition of "trap" is applied for pipe walls. To include value of instantaneous fluctuating flow velocity on trajectory of particles, Discrete Random Walk Model (DRWM) is employed with time scale constant of 0.3, recommended for Reynolds Stress Model (RSM) by Ansys Fluent user's guide. For sake of brevity complete description of this method is not described here.

The deposition efficiencies have been presented as a function of stokes number. Stokes number is a frequently used dimensionless parameter that is interpreted as the particle response time to the response time of system (fluid flow in this paper) and is expressed as:

$$st = \frac{\tau_D}{t_s} \tag{8}$$

where

$$\tau_D = \frac{\rho_p {d_p}^2}{18\mu} \tag{9}$$

and

$$t_s = \frac{L_s}{V_s} \tag{10}$$

where τ_D is particle response time, t_s is fluid response time, ρ_p is density of particle, d_p is particle diameter, μ is the fluid viscosity, L_s is characteristic length, and V_s is characteristic velocity. Based on the study of Pui et al., radius of pipe and flow axial velocity have been used as the characteristic length and characteristic velocity. To improve clarity, Table 2 lists the important parameters used in these simulations.

Deposition efficiency (η) is calculated by dividing mass of the particles deposited on the bend wall to the total mass of the particles that have entered the bend. As particles at each injection have uniform size and density, mass is replaced with number of particles to derive deposition efficiency which becomes ratio of number of particles deposited on bend wall to total number of particles that have entered the bend:

$$\eta = \frac{N_{bend}}{N_{total}} \tag{11}$$

Table 2
List of important parameters used in this work.

Particle diameter range (d_p)	2 μm to 9 μm	Range of *St* number	0.1 to 1.05
Pipe diameter (d)	8.51 mm	Flow Reynolds number (*Re*)	10,000
Vanes' heights (h/d)	0.05, 0.1, 0.15, 0.2, 0.25, 0.3, 0.35	Curvature ration (δ)	5.6
Swirling pitch (P)	0.15 m, 0.1 m, 0.075 m, 0.05 m	Particle density (ρ_p)	895 kg/m^3

3. Results and discussion

3.1. Problem validation

Experimental work of Pui et al. has been employed to validate the CFD simulation. They used monodispersed aerosols generated by the vibrating orifice aerosol generator. The aerosols were generated using oleic acid ($\rho = 895$ kg/m^3). As liquid aerosols were used in the tests it was assumed that once the particles impact the walls there is no particle bounce and all aerosols adhere to it. As mentioned before the boundary condition for discrete phase at the pipe walls were set to "trap" to provide same status as the experimental tests. According to Pui et al. the bends were preceded by a sufficiently long entrance so the fully developed profile was obtained before the bend. To mimic the same conditions a long entrance was considered for this study based on the Eq. (1) to have fully developed flow at the entrance of the bend.

Fig. 5 shows the numerical and experimental results of particle deposition efficiency as a function of stokes number. As shown in the figure, numerical results are in good agreement with the experimental data and a maximum deviation of 6.5% is observed at st = 0.01 which shows the accuracy of the method used for simulations.

3.2. Swirl number

To investigate effect of swirl on deposition of particles the swirling number has been used to quantify swirl intensity. The values of swirling numbers are shown in Fig. 6 as a function of spiral vanes' heights for different swirling pitches. Higher spiral vanes with shorter swirling pitches engage more volume fraction of fluid with the blades and thus raise the swirl intensity. However the diagram shows that swirl number is not linearly proportional to the height of vanes. After an optimum point further increment of vanes' height doesn't result in more growth of swirling number to a point that raising vane height doesn't result a significant impact on the swirling number and this conclusion is valid for all pitches.

Despite imposing swirl to the fluid flow, the guiding vanes have also an undesirable effect on pressure drop along the pipe which means the losses must be considered for employing an efficient swirl generator. Pressure coefficient is a dimensionless parameter used to study relative pressure in a domain and is derived by the Eq. (12).

$$C_p = \frac{P_l - P_\infty}{\frac{1}{2}\rho u_\infty{}^2} \tag{12}$$

where P_l is the pressure of the point at which C_p is being calculated and P_∞ and u_∞ are the pressure and velocity of a reference point and ρ is the density of fluid. Fig. 7 shows pressure coefficient for different swirl generators with various guiding vanes and swirling pitches. The data for reference values have been extracted from the point located on the central axis of pipe at the inlet of the swirling section and C_p is calculated on the central axis of pipe at the outlet of the swirling section. As it is predictable raising amount of h/d and lowering pitch length results in reduction of C_p which means higher swirl intensity is associated with extra pressure drop along the pipe however the graph shows that for $P = 0.05$ m the gradient is more severe.

3.3. Flow patterns

Flow pattern in the bend is presented at cross sections with bend deflections of $\theta = 0^\circ, 30^\circ, 45^\circ, 60^\circ, 90^\circ$ in Fig. 8. To show effect of swirl on flow patterns, streamlines of flow at low to high swirling numbers are depicted along with streamlines of a simple pipe for comparison. The color spectrum in background of the streamlines shows velocity magnitude. In the simple pipe the secondary flows form symmetrical vortices which were first observed by Dean [28]. This is due to the fact that presence of bend forces the moving fluid at the center of the pipe toward the wall and the fluid near the wall tends to move toward the center of the pipe instead, and this displacement of fluid resulted from centrifugal force creates C shaped vertical streamlines called Dean vortices. However when the swirl is imposed to flow these symmetrical patterns disappear at the bend entrance until the pressure gradients due to centrifugal force dominates the swirl and reform the so-called Dean vortices. Astute analysis of the figure highlights the fact that higher swirl intensities postpone reformation of Dean vortices. For lower swirl numbers such as $S_n = 0.03118$ the Dean vortices reformation takes place at $\theta = 15^\circ$. For $S_n = 0.1434$ it is seen that at $\theta = 30^\circ$ Dean vortices start to reappear and for

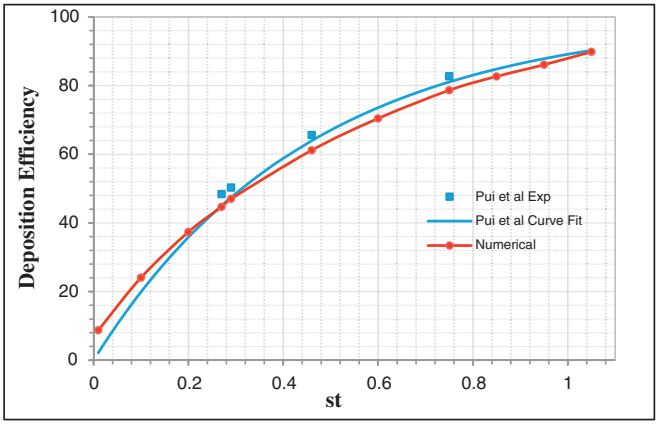

Fig. 5. Problem validation: Comparison of deposition efficiency between experimental work of Pui et al. and the present numerical simulation.

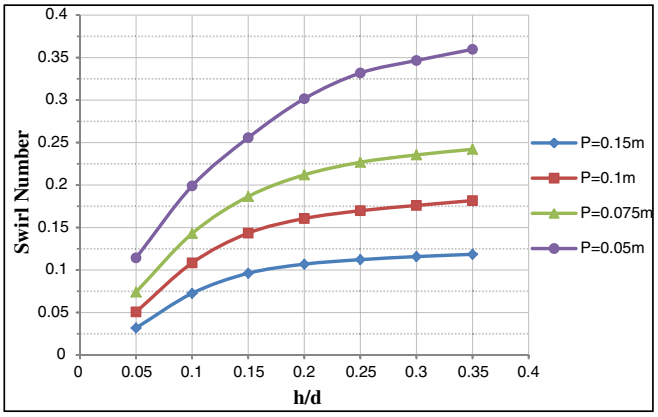

Fig. 6. Swirl numbers for different swirling pitches and spiral vanes' heights.

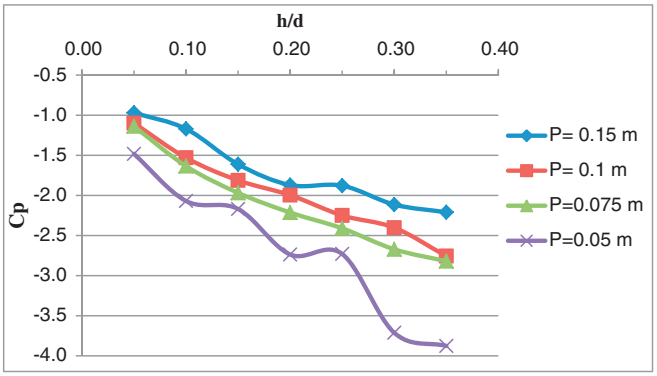

Fig. 7. Pressure coefficient for different pitches and vanes' heights.

$S_n = 0.2421$ this happens at $\theta = 60^{\circ}$. It is to be noted that at higher swirl numbers like $S_n = 0.3597$ (the highest swirl number achieved in these simulations) the imposed swirling flow by swirl generators keep their dominance until the bend outlet section and no Dean vortices are observed throughout the bend. These flow patterns are compatible with findings of Kalpakli [29] who experimentally investigated the turbulent flow downstream of a 90° bend in the presence of swirling flow.

3.4. Deposition efficiency

Deposition efficiencies are presented as a function of stokes number in Fig. 9. These curves show deposition rates at different swirling pitches for different amounts of h/d. It is found that deposition rate of particles on the bend walls reduces at each step of increasing guiding vanes' height and this is true almost for all swirling pitches. It can be concluded that taking only the effect of swirl into account without comparing the results to the simple pipe, higher swirl intensities reduce deposition rate but comparing the results with deposition rates derived from simple pipe shows that swirling flow may also increase deposition rate.

Fig. 9a indicates deposition efficiencies for $P = 0.15$ m. It is shown that for lower stokes numbers, when comparing with simple pipe, exerting swirl to flow using guiding vanes with height of $h/d = 0.05$ to $h/d = 0.1$ raises deposition rate but further increment of swirl intensity by raising h/d reduces the deposition rate below the simple pipe and this is true for stokes numbers ranging from $st = 0.1$ to $st = 0.46$. For stokes numbers greater than $st = 0.46$, generation of swirl with any intensity reduces the percentage of deposits. In Fig. 9b the results are shown for $P = 0.1$ m which are largely similar to the results for $P = 0.15$ m.

In Fig. 9c which is for $P = 0.075$ m, again there are some similarities in deposition tendency of particles but also some major differences are observed. The range of stokes numbers in which imposing swirl causes

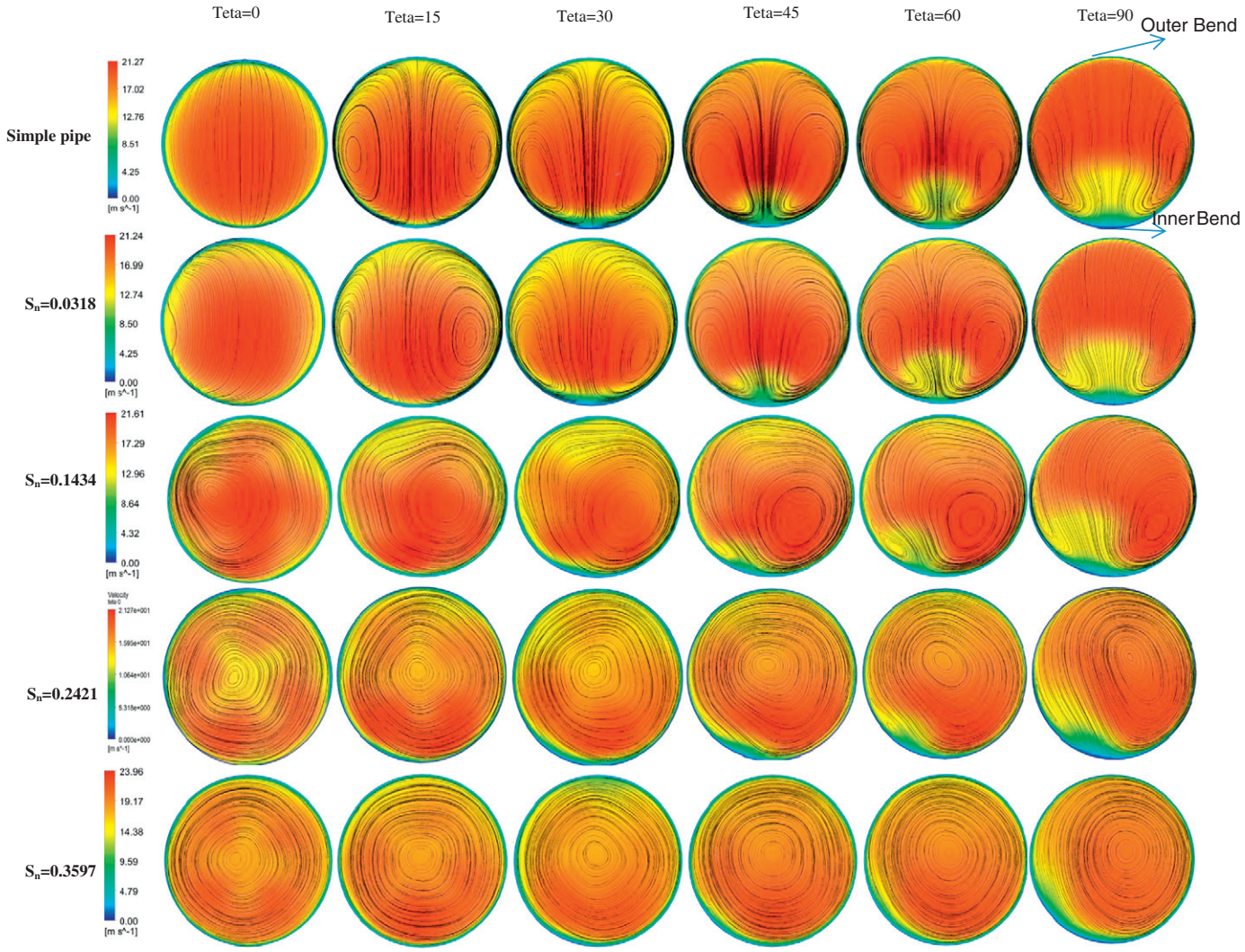

Fig. 8. Flow streamlines in simple pipe and in swirling flow with swirl numbers of $S_n = 0.0318$, $S_n = 0.1434$, $S_n = 0.3597$ at cross sections with bend deflections of $\theta = 0^{\circ}, 30^{\circ}, 45^{\circ}, 60^{\circ}, 90^{\circ}$.

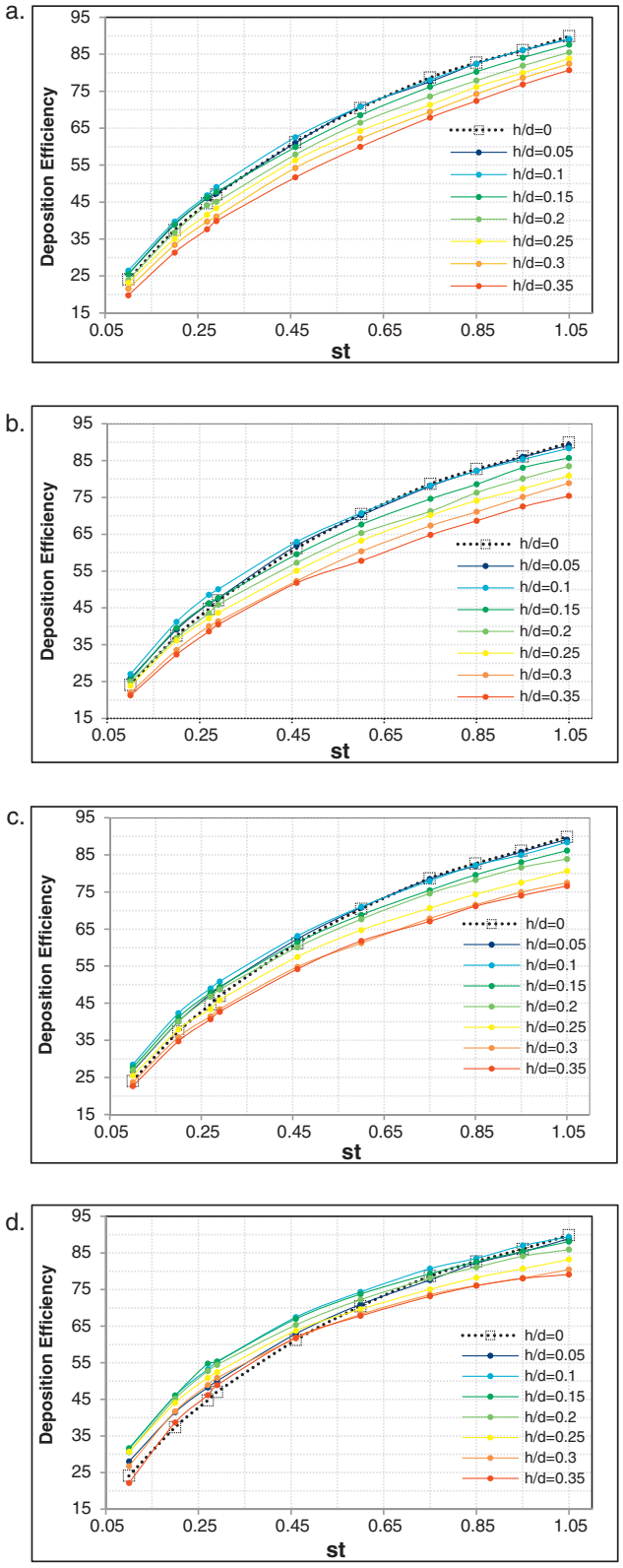

Fig. 9. Deposition efficiencies as function of stokes number for different guiding vanes and swirling pitches: (a) $P = 0.15$ m, (b) $P = 0.1$ m, (c) $P = 0.075$ m, (d) $P = 0.05$ m.

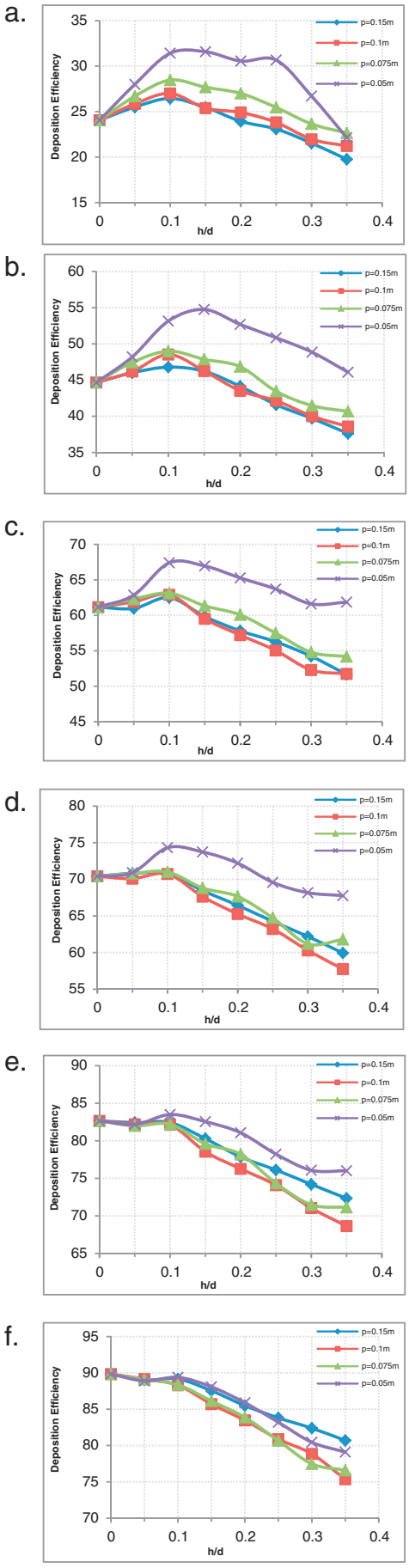

Fig. 10. Deposition efficiencies for different stokes numbers in separate charts: (a): st = 0.1, (b): st = 0.27, (c): st = 0.46, (d): st = 0.6, (e): st = 0.85, (f): st = 1.05.

groth in deposition efficiency is between st = 0.1 to st = 0.75. It means that for particles up to st = 0.75 swirl raises deposition of particles and for higher stokes numbers (greater than st = 0.75) swirl reduces deposition efficiency. This range for the shortest pitch, $P = 0.05$ m (Fig. 9d) is between st = 0.1 to st = 1.05 which means particles with a wide variety of stokes numbers grow in deposition rate when being exposed to swirl and reduction of deposition happens for larger particles such as st = 1.05. For better indication of the conclutions made, the data of Fig. 9 have been rearranged to show deposition for different stokes numbers separately. In Fig. 10a-f deposition rates for small to large particles (st = 0.1,0.27,0.46,0.6,0.85 and 1.05) are displayed as function of (h/d) for different pitches. These results show that swirl generated by shorter pitches for a wider range of stokes numbers and swirl intensities, raises deposition rates unlike the longer pitches that tend to decrease the deposition rates in wider range of swirl intensities and stokes numbers.

The greatest amount of reduction in deposition with comparing to simple pipe is about 15% and occurs for st = 1.05 at $P = 0.1$ m for h/d = 0.35 which generates swirl intensity of Sn = 0.1817. And the greatest amount of deposition increment is 10% which relates to $P = 0.05$ m and h/d = 0.15 for st = 0.27.

This behavior can be justified through Fig. 11 where turbulent intensity of flow at the inlet of bend is depicted against the height of spiral vanes. The quantities for the curves have been derived by integrating this parameter over the bend inlet surface ($\theta = 0^{\circ}$). As mentioned before by raising spiral vanes' heights, deposition rate increases at first but later, it decreases. Also for particles with lower stokes numbers (Fig. 10a–c) an extremum is observed at h/d = 0.1 but this extremum evades gradually when moving from lower stokes numbers to higher ones. The same trend is observed in Fig. 11 where it shows an extremum at h/d = 0.1 for all pitches. By comparing Figs. 10 and 11, one can find that there is very close relation between the deposition rate of smaller particles and the turbulent intensity of flow. It can be concluded that motion of smaller particles is more affected by turbulent intensity in comparison with larger particles. It is to be noted that there is one exception in Fig. 10a that there are two extremums at h/d = 0.25. As this behavior (second extremum) is not repeated for other stokes numbers and the difference between deposition efficiency of two consecutive points is <1% it doesn't seem to have any meaningful explanation.

These results show that although lowering pitch of swirling section raises swirl intensity but is not a definite method to reduce deposition rate. As shown in Fig. 10 particles with lower stokes numbers increase in deposition rate when being imposed to swirl but as the swirl is intensified with raising vanes' heights the deposition rate decreases. This oscillation in deposition happens for a wider range of stokes numbers when using lower pitches. On the other hand it can be seen that larger particles have uniform and predictable behavior to swirl generation in pipe bends. For example as indicated in Fig. 10 deposition of particles with st = 1.05 which is the highest stokes number simulated in this work, decreases at all swirling pitches and guiding vanes. This outcome is confirmed in Fig. 12 where distribution of particles at bend deflection of $\theta = 90^{\circ}$ is displayed for st = 0.1, 1.05 in a simple pipe flow and in a swirling flow with $S_n = 0.3597$. Sampling of particles at this section started with start of particle injection to the computational domain

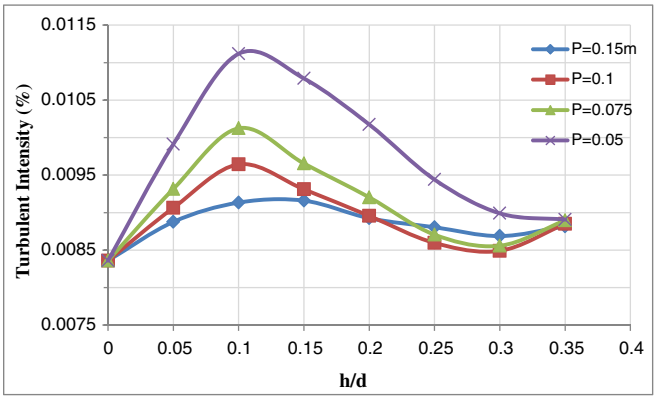

Fig. 11. Turbulent intensity at the bend inlet section ($\theta = 0$) for different swirling pitches and spiral vanes' heights.

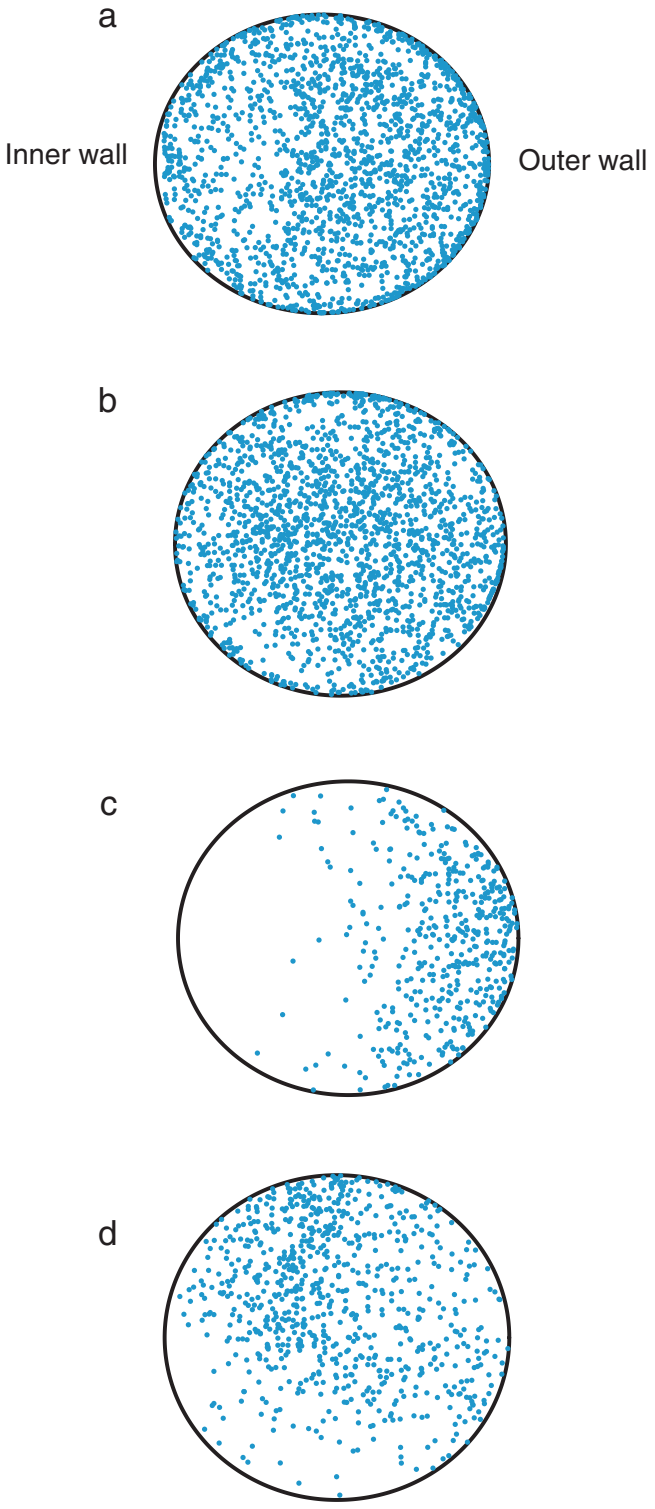

Fig. 12. Distribution of particles on the bend outlet section ($\theta = 90^{\circ}$) for (a): st = 0.1, simple pipe, (b): st = 0.1, $S_n = 0.3597$ (c): st = 1.05, simple pipe, (d): st = 1.05, $S_n = 0.3597$. Positions of outer wall and inner wall are shown in the figure.

and after all particles either trapped on the bend wall or escaped the bend outlet, sampling was stopped.

In Fig. 12b particles are more concentrated at the center of pipe as a result of swirling flow. Also there is a thin layer of particles concentrated adjacent to the outer bend wall in Fig. 12a which is not seen in Fig. 12b. Despite slight differences mentioned, comparison of Fig. 12a–b reveals that swirl doesn't considerably influence distribution and deposition of smaller particles and the aforementioned results confirm this conclusion. However Fig. 12c–d show there is significant difference in behavior of large particles when being imposed to swirl. As shown in this figure, in simple pipe particles are more concentrated near the outer wall region but in swirling flow particles have almost uniform distribution all over the surface. In flow through a bend, small particles have less inertia that can easily follow the flow streamlines and penetrate bend but larger particles have larger centrifugal force upon them which doesn't allow them to easily follow the curved streamlines and separate from the flow and finally deposit on the outer bend wall. When larger particles are exposed to swirling flow it dominates the centrifugal force and keeps the particles away from wall and reduces deposition rate as a consequence.

4. Conclusions

Discrete Phase Model (DPM) was used to simulate deposition of particles with diameters ranging from 2 to 9 μm and effect of swirl imposed by internal spiral vanes was investigated on the deposition efficiency. Different swirling pitches and vanes' heights were tested in this study and the swirl intensities were reported by dimensionless parameter, swirl number. It was found that increasing vanes' heights doesn't linearly increase swirl intensity and after a point, there is no significant change in swirl intensity by further increment of vanes' heights. Both increasing vanes' heights and lowering swirling pitch raise swirl intensity, however if swirl generator is needed for reducing deposition efficiency of particles, it should be noted that increasing vanes' heights has better effect in comparison with lowering swirling pitch. The results showed that for particles with lower stokes numbers imposing swirl raises deposition efficiency at first and later with increasing swirl intensity deposition efficiency reduces. For larger stokes numbers any amount of swirl intensity reduces deposition efficiency and this shows that larger particles have more predictable behavior when being imposed to swirl. It was also found that motion of particles with lower stokes numbers is more affected by turbulent intensity and increasing turbulent intensity also increases deposition of particles with lower stokes numbers.

References

[1] B.Y.H. Liu, J.K. Agarwal, Experimental observation of aerosol deposition in turbulent flow, J. Aerosol Sci. 5 (1973) 145–155.
[2] W.-C. Yang, Estimating the solid particle velocity in vertical pneumatic conveying lines, Ind. Eng. Chem. Fundam. 12 (1973) 349–352.
[3] M. Alonso, M. Carsí, C.H. Huang, Using the fully developed concentration profile to determine particle penetration in a laminar flow tube, J. Aerosol Sci. 97 (2016) 34–37, http://dx.doi.org/10.1016/j.jaerosci.2016.04.002.
[4] P. Armand, D. Boulaud, M. Pourprix, J. Vendel, Two-fluid modeling of aerosol transport in laminar and turbulent flows, J. Aerosol Sci. 29 (1998) 961–983, http://dx.doi.org/10.1016/S0021-8502(98)00006-8.
[5] X. Luo, S. Yu, Deposition of particles in turbulent pipe flow, China Particuology 4 (2006) 31–34, http://dx.doi.org/10.1016/S1672-2515(07)60230-9.
[6] A. Dehbi, A CFD model for particle dispersion in turbulent boundary layer flows, Nucl. Eng. Des. 238 (2008) 707–715.
[7] Y.S. Cheng, C.S. Wang, Motion of particles in bends of circular pipes, Atmos. Environ. 15 (1981) 301–306, http://dx.doi.org/10.1016/0004-6981(81)90032-9.
[8] D.Y.H. Pui, F. Romay-Novas, B.Y.H. Liu, Experimental study of particle deposition in bends of circular cross section, Aerosol Sci. Technol. 7 (1987) 301–315, http://dx.doi.org/10.1080/02786828708959166.
[9] K. Sun, L. Lu, H. Jiang, A numerical study of bend-induced particle deposition in and behind duct bends, Build. Environ. 52 (2012) 77–87, http://dx.doi.org/10.1016/j.buildenv.2011.12.009.
[10] R. Gao, A. Li, Dust deposition in ventilation and air-conditioning duct bend flows, Energy Convers. Manag. 55 (2012) 49–59, http://dx.doi.org/10.1016/j.enconman.2011.10.018.
[11] L. Hongtao, Z. Li, Prediction of particle deposition characteristic in 90° square bend: square bend particle deposition characteristic, Appl. Therm. Eng. 31 (2011) 3402–3409.
[12] M. Breuer, H.T. Baytekin, E.A. Matida, Prediction of aerosol deposition in 90° bends using LES and an efficient Lagrangian tracking method, J. Aerosol Sci. 37 (2006) 1407–1428.
[13] P. Zhang, R.M. Roberts, A. Bénard, Computational guidelines and an empirical model for particle deposition in curved pipes using an Eulerian-Lagrangian approach, J. Aerosol Sci. 53 (2012) 1–20.
[14] Q. Li, J. Song, C. Li, Y. Wei, J. Chen, Numerical and experimental study of particle deposition on inner wall of 180° bend, Powder Technol. 237 (2013) 241–254, http://dx.doi.org/10.1016/j.powtec.2012.11.008.
[15] K.J. Hanley, E.P. Byrne, K. Cronin, Probabilistic analysis of particle impact at a pipe bend in pneumatic conveying, Powder Technol. 233 (2013) 176–185.
[16] C.B. Solnordal, C.Y. Wong, J. Boulanger, An experimental and numerical analysis of erosion caused by sand pneumatically conveyed through a standard pipe elbow, Wear 336 (2015) 43–57.
[17] L. Xu, Q. Zhang, J. Zheng, Y. Zhao, Numerical prediction of erosion in elbow based on CFD-DEM simulation, Powder Technol. 302 (2016) 236–246, http://dx.doi.org/10.1016/j.powtec.2016.08.050.
[18] R. Macchini, M.S.A. Bradley, T. Deng, Influence of particle size, density, particle concentration on bend erosive wear in pneumatic conveyors, Wear 303 (2013) 21–29, http://dx.doi.org/10.1016/j.wear.2013.02.014.
[19] J. Oh, S. Choi, J. Kim, Numerical simulation of an internal flow field in a uniflow cyclone separator, Powder Technol. 274 (2015) 135–145, http://dx.doi.org/10.1016/j.powtec.2015.01.015.
[20] W. Duangthongsuk, S. Wongwises, An experimental investigation of the heat transfer and pressure drop characteristics of a circular tube fitted with rotating turbine-type swirl generators, Exp. Thermal Fluid Sci. 45 (2013) 8–15, http://dx.doi.org/10.1016/j.expthermflusci.2012.09.009.
[21] A.D. Rocha, A.C. Bannwart, M.M. Ganzarolli, Numerical and experimental study of an axially induced swirling pipe flow, Int. J. Heat Fluid Flow 53 (2015) 81–90, http://dx.doi.org/10.1016/j.ijheatfluidflow.2015.02.003.
[22] J. Zhou, C. Du, S. Liu, Y. Liu, Comparison of three types of swirling generators in coarse particle pneumatic conveying using CFD-DEM simulation, Powder Technol. 301 (2016) 1309–1320.
[23] H.U.I. Li, Characteristics of a horizontal swirling flow pneumatic conveying with a curved pipe, Part. Sci. Technol. 18 (2000) 187–198, http://dx.doi.org/10.1080/02726350008906835.
[24] B.R. Munson, D.F. Young, T.H. Okiishi, Fundamentals of fluid mechanics, Oceanogr. Lit. Rev. 10 (1995) 831.
[25] A.F.U. Guide, Release 15.0. 2015, (n.d.).
[26] M.A. Habib, D.M. McEligot, Turbulent heat transfer in a swirl flow downstream of an abrupt pipe expansion, Heat Transf., Vol. 3, 1982, pp. 159–164.
[27] W.C. Hinds, Aerosol Technology: Properties, Behavior, and Measurement of Airborne Particles, John Wiley & Sons, 2012.
[28] W.R. Dean, XVI. Note on the motion of fluid in a curved pipe, London, Edinburgh, Dublin Philos. Mag. J. Sci., 4, 1927, pp. 208–223.
[29] A. Kalpakli, R. Örlü, Turbulent pipe flow downstream a 90° pipe bend with and without superimposed swirl, Int. J. Heat Fluid Flow 41 (2013) 103–111, http://dx.doi.org/10.1016/j.ijheatfluidflow.2013.01.003.